EFFICIENCY OPTIMIZED CONTROL OF PERMANENT-MAGNET SYNCHRONOUS MOTORS FOR ELECTRIC VEHICLES OVER THE ENTIRE-SPEED RANGE

Hanaa ELSHERBINY[1], Mohamed Kamal AHMED[2], Mahmoud A. ELWANY[3]

The Interior Permanent magnet synchronous motors (IPMSMs) are widely used as the main drive for electric vehicle (EV) propulsion. High efficiency of the motor and power converter is essential as they consume most of battery power. This paper presents an optimization-based method aiming to achieve the maximum system efficiency including IPMSM and power converter. The method is applicable over the entire speed range. It involves the field weakening (FW) control scheme. To accurately estimate the overall system efficiency, First, a high-fidelity machine model considering the magnetic saturation, spatial harmonics, and iron loss effect is built. The magnetic characteristics of simulated 12/10 IPMSM is generated precisely using the Finite Element Analysis (FEA). Then, an inverse solution of flux-linkages is extracted to simplify the model as well as to avoid the derivative calculations. Second, a detailed analysis and estimation of system losses are achieved. The system losses include the fundamental copper and iron losses, harmonic copper and iron losses, inverter losses (conduction and switching losses), and mechanical losses. The loss models are included within motor model through MATLAB Simulink environment. Third, a searching algorithm is developed to define the best current angle for maximum efficiency per ampere (MEPA) control. The same algorithm is also used to define the best current angle for maximum torque per ampere (MTPA) control. The MTPA control is used for comparisons and investigations. Finally, a series of results is conducted to show the effectiveness and fidelity of the proposed MEPA control.

Keywords: interior permanent magnet synchronous motors, finite element analysis, iron losses, inverter losses, MEPA, MTPA.

1. Introduction

The Electric vehicles (EVs) are a direct way for establishing a low-carbon economy. They are gaining an increased popularity because of their advantages[1]–[3]. They offer no emissions, low maintenance, low cost, and

[1] Assistant Lecturer, Electrical Engineering Department, Faculty of Engineering, El-Azhar University, Cairo, Egypt, e-mail: hanaa.elsherbiny90@gmail.com
[2] Prof., Electrical Engineering Department, Faculty of Engineering, El-Azhar University, Cairo, Egypt, e-mail: MohamedMahmoud51.el@azhar.edu.eg
[3] Prof., Electrical Engineering Department, Faculty of Engineering, El-Azhar University, Cairo, Egypt, e-mail: elwany60@hotmail.com

safety drive [4]–[6]. For an EV, most of the battery power is consumed by the main drive system that includes the motor and power converter. Therefore, the efficiency optimization of EVs drive system has a great attention from researchers [7].

Interior Permanent magnet synchronous motors (IPMSMs) have the best overall performance as the main drive system in EVs[2], [8]. This is mainly due to their superiorities such as small weight and size, wide speed range, high power density, low noise, and high efficiency. However, improving the efficiency of IPMSM drive system especially for EVs has received considerable research interests to increase the drive milage per battery charge.

The improvement of motor efficiency can be achieved by the machine design and/or drive control. First, on the machine design stage, new configurations for the stator and rotor with novel design procedures are employed to improve motor efficiency[9], [10]. Besides, optimal design and control of power converter can improve the system efficiency[11], [12]. Second, on the control stage, the maximum torque per ampere (MTPA) and maximum efficiency per ampere (MEPA) control are the latest advanced control for improving the drive performance [1], [7], [13]. The MTPA control has been developed by the improvement of analytical models [12], [14], online parameter estimation methods[15], and virtual signal injection methods [17]–[19]. However, the MTPA control aims basically to reduce only the copper losses in PMSM [20]. The MTPA control does not consider the other losses such as the stator iron loss and rotor eddy current loss. The iron losses are significant and cannot be ignored, especially under high–speeds [5], [21]–[23]. Besides, the MTPA control is only applicable over a limited speed range. In addition, the field weakening control has to be included above the base speed [3].

On the other side, the MEPA can consider the iron losses. Besides, the other system losses such as the inverter losses, mechanical losses, and harmonic iron and copper losses can be included within the control algorithm. This, in turn, helps to accurately estimate and improve the overall system efficiency [24]. In [8], [24], [25], the fundamental iron losses are considered to maximize the system efficiency. However, harmonic iron losses are not considered which affect the motor efficiency. Further efficiency improvement can be achieved by the consideration of fundamental and harmonic iron losses, especially in the high–speed and light load regions [7].

The calculation of losses, system efficiency, and optimal current references depends basically on system modeling. The IPMSMs have highly nonlinear characteristics due to magnetic saturation, reluctance torques, and spatial harmonics [20], [26]. The reluctance torques cause highly nonlinear relationship between torque and armature current. The spatial harmonics in phase-voltages appears as a result of reluctance torques and variation of magnetic energy

with rotor position [27], [28]. For proper efficiency control, the motor model must include the effects of saturation and spatial harmonics. Also, the iron losses (fundamental and harmonic) must be included as they affect output torque. In addition, for EVs, improving the overall system efficiency is more important compared to motor efficiency. Therefore, including the inverter losses is essential.

This paper presents an efficiency optimization procedure for the IPMSMs in EVs. First, a high-fidelity machine model that considers magnetic saturation, spatial harmonics, and iron loss effect is accurately built. The Finite Element Analysis (FEA) is employed to calculate the machine characteristics. The FEA considers accurately the saturation and spatial harmonics as well as cross-coupling. The model is built using an inverse solution of flux-linkage to obtain the currents. This is done to simplify the modeling and to avoid the derivative calculation. Second, the motor loss considering fundamental and harmonic iron losses, copper loss, mechanical loss, as well as the inverter losses are employed to accurately calculate the total system efficiency. Third, a searching algorithm has been developed to derive the optimal current angles, and hence the optimal efficiency over the entire speed range. Finally, a comparison between the proposed MEPA and the conventional MTPA techniques is given. The paper organization is done as follows: a high-fidelity machine model is summarized in Section 2 including the results of FEA and the inverse solution of currents versus flux-linkages. Section 3 shows the detailed analysis of system losses. Section 4 gives the MTPA and MEPA operations for IPMSMs. The optimization procedure is given in Section 5. The simulation results and their discussions are in Section 6. Finally, Section 7 is the conclusion of this research.

2. High-Fidelity Modeling of IPMSM

The modeling of an IPMSM can be represented by Equations (1) - (3).

$$v_d = R_s i_d + \frac{d\lambda_d}{dt} - \omega\lambda_q; \quad v_q = R_s i_q + \frac{d\lambda_q}{dt} + \omega\lambda_d \tag{1}$$

$$T_e = \frac{3}{2} p i_q \left(\lambda_d i_q - \lambda_q i_d\right) \tag{2}$$

$$J\frac{d\omega}{dt} = T_e - T_L - B\omega \tag{3}$$

where v_d and v_q are d and q-axis components of voltage, i_d and i_q are d and q-axis components of armature current, λ_d and λ_q are d and q-axis components of flux-linkage, R_s is the stator resistance, ω is the electrical angular speed, T_e is the motor torque, p is the number of pole pairs, J is the inertia, B is the frictional coefficient, and T_L is the load torque.

The effect of magnetic saturation and spatial harmonics can be included if the *d*- and *q*-axis flux-linkages λ_d, λ_q become functions in *d*- and *q*-axis currents i_d, i_q and rotor position θ_i. Thus, a machine model based on flux-linkages can be given by Equation (4). The electromagnetic torque, obtained from FEA, can be also described as a function of i_d, i_q, and θ_i as given by Equation (5). This representation considers all the torque components as well as the cogging torque.

$$\lambda_d = f(i_d, i_q, \theta_i); \quad \lambda_q = g(i_d, i_q, \theta_i) \tag{4}$$

$$T_e = T(i_d, i_q, \theta_i) \tag{5}$$

For MTPA and MEPA control, the cost function is the average torque and efficiency, respectively. The efficiency estimation requires the calculation of average torque. Hence, the average flux-linkages and torque are used to model the IPMSM. They are given by Equation (6).

$$\begin{aligned} \lambda_{d\_avr}(i_d, i_q) &= \frac{\sum_{i=0}^{N} \lambda_d(i_d, i_q, \theta_i)}{N+1} \\ \lambda_{q\_avr}(i_d, i_q) &= \frac{\sum_{i=0}^{N} \lambda_q(i_d, i_q, \theta_i)}{N+1} \\ T_{e\_avr}(i_d, i_q) &= \frac{\sum_{i=0}^{N} T_e(i_d, i_q, \theta_i)}{N+1} \end{aligned} \tag{6}$$

The flux-linkages are obtained by integrations as illustrated in Equation (7).

$$\begin{aligned} \lambda_d &= \int (V_d - R_s i_d + \omega \lambda_q) dt \\ \lambda_q &= \int (V_q - R_s i_q - \omega \lambda_d) dt \end{aligned} \tag{7}$$

By performing inverses of Equation (6), the d- and q-axis currents are determined by Equation (8).

$$i_d = f^{-1}(\lambda_d, \lambda_q); \quad i_q = g^{-1}(\lambda_d, \lambda_q) \tag{8}$$

Fig. 1 shows the IPMSM model. The model is built based on the Equation (1) – (5). The inputs are the d- and q-axis voltages (v_d, v_q). The voltages are employed to estimate the d- and q-axis flux-linkages (λ_d, λ_q) using Equation (7). Then, the d- and q-axis currents (i_{da}, i_{qa}) are calculated based on the flux inverse model that is given by Equation (8). The iron losses are represented by the currents i_{df} and i_{qf}. The motor electromagnetic torque is estimated uaing Equation (5) as a function of i_{da} and i_{qa} currents. Noting that the model involves not only the magnetic saturation and spatial harmonic effects but also the iron loss effect.

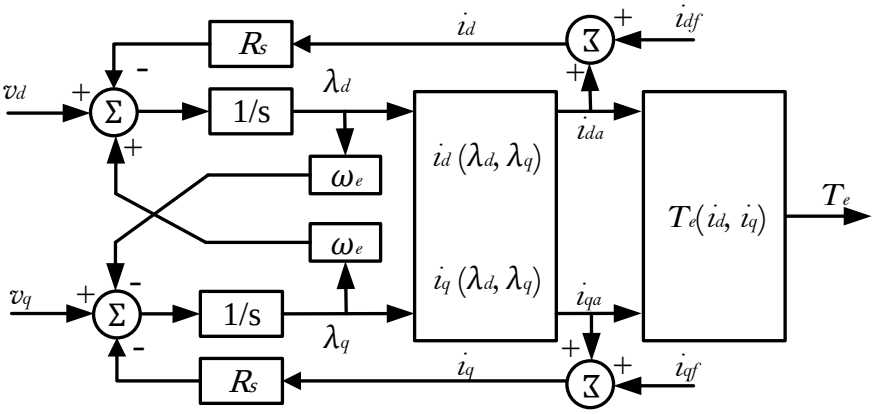

Fig. 1. The schematic of IPMSM model.

2.1. Finite Element Analysis (FEA) of IPMSM

The FEA is widely accepted for performance evaluation and characteristics calculation of complex structures such as IPMSMs. The FEA is an accurate numerical method to estimate flux-linkage in each stator pole, developed torque, and self and mutual inductances. Lately, the computations of FEA are speeded up using the static magnetic field analysis [29]. Although the FEA offers higher accuracy compared to normal analytical methods, it needs the exact geometrical parameters and material properties. However, it presents a robust method to verify along with the obtained experimental results [29].

High accuracy magnetic characteristics can be obtained using FEA by proper calibration with the experimental machine. The calibration procedure includes a simple no-load and load tests. First, the no-load voltages, preferred at high speeds, are used to accurately estimate the permanent magnet (PM) flux-linkage. Then, the coercivity of the PM material can be adjusted within FEA to produce the same no-load voltages. Probably, it will be decreased a bit lower than the manufacturer datasheets due to the manufacturing tolerances [27]. Second, the loading test can be done under motoring action. The motor is operated with a known d- and q-currents. Then, the developed torque is measured and compared to the estimated torque via FEA. The difference, if exists, can be adjusted by the BH curve of magnetic steel material. Once, the calibration procedure is completed, the FEA can produce the precise machine characteristics to be employed in machine modeling.

Table 1 gives the structural dimension of studied 12/10 IPMSM. It also gives the inverter details that are used in further analysis. Fig. 2 shows the FEA flux lines and flux density distribution with i_q=10A, i_d=-4A, and rotor position angle θ_i= $\underline{0}^{\circ}$. As noted the stator pole shoes and rotor rips have the highest flux densities. They are in deep saturation. Including of such details using analytical

methods is a very complicated task with a questioned degree of accuracy. Despite the small volume of pole shoes and rotor rips, they affect the motor performance.

Fig. 3 shows the flux-linkages ($\lambda_d(i_d, i_q)$, $\lambda_q(i_d, i_q)$) and torque $T_e(i_d, i_q)$ as functions of i_d and i_q. These data are obtained via FEA by varying i_d from -25 to 0 A in steps of 1A, i_q is changed from from 0 to 25 A in steps of 1A, and θ_i is varied from 0˚ (d-axis) to 72˚ (q-aixs) insteps of 1˚ (mech. degree). Then, the average flux-linkages and torque are obtained according to Equation (6). As seen, the flux linkages and torque show nonlinear relations with current.

2.2. Inverse Solution of Currents versus Flux-linkages

The direct and quadrature currents (i_d, i_q) can be found based on the λ_d (i_d, i_q) and λ_q (i_d, i_q) maps. The solution of the inverse problem, in Equation (6), can be obtained by minimizing the folowing objective function F_{obj}.

Table 1

The major parameters of IPMSM and inverter

Motor Parameters		Inverter Parameters	
Parameter	Value	Parameter	Value
No. of rotor poles	10	V_{ceo}	1.7 V
Power	1.2 kW	V_{Do}	1.6 V
DC link voltage	200 V	R_o	0.17 mΩ
Rated torque	5 Nm	R_D	0.16 mΩ
Base speed	1500 r/min	e_{on}	350 µJ
Number of slots	12	e_{off},	175 µJ
Stator outer diameter	120 mm	e_{rr}	50 µJ
Rotor outer diameter	74 mm	V_{nom} / I_{nom}	600V/20A

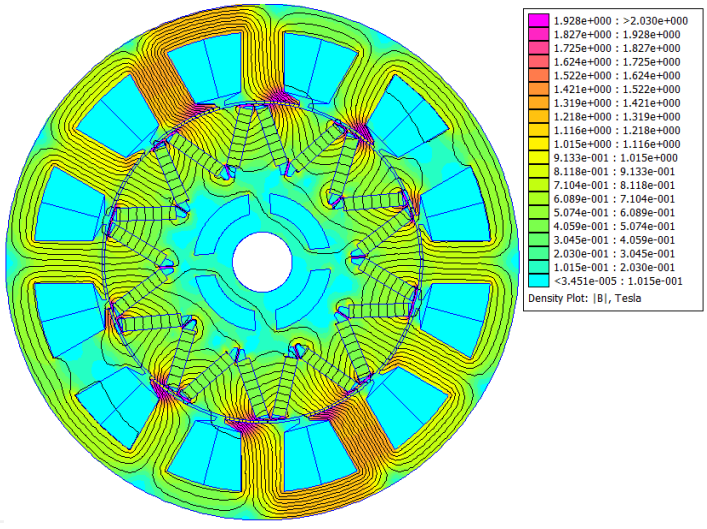

Fig. 2. The FEA flux lines and flux density at i_q=10A, i_d=-4A and θ_i= 0˚.

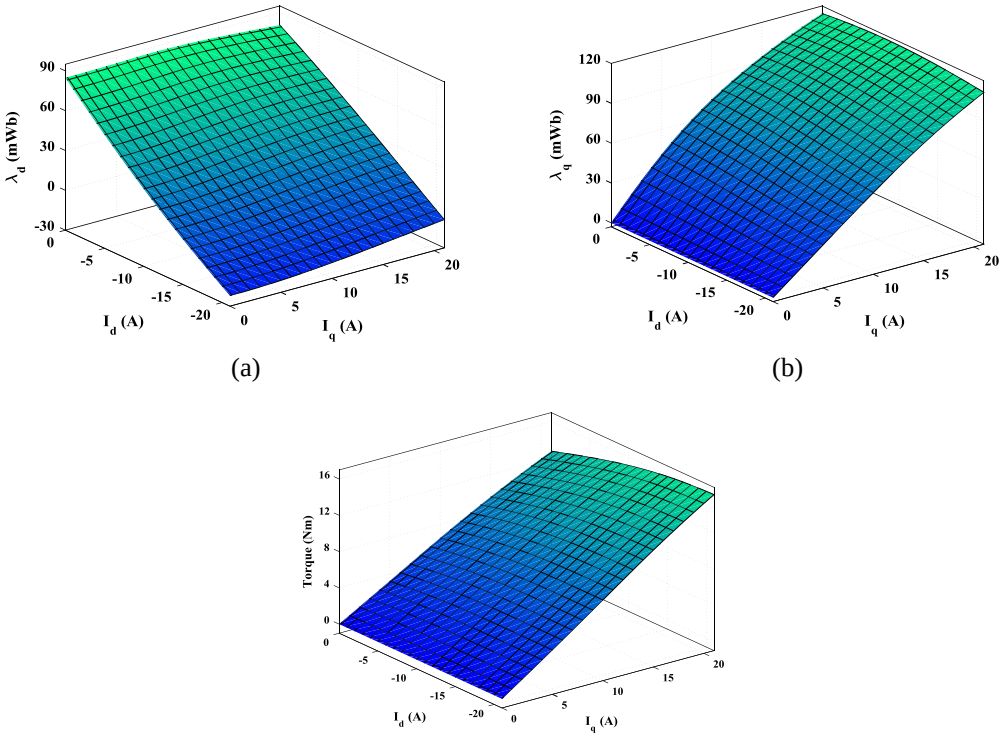

Fig. 3. The FEA-calculated (a) d-axis flux, (b) q-axis flux, (c) torque.

$$F_{obj}(i_d, i_q) = min\{|\lambda_d(i_d, i_q) - \lambda_{do}| + |\lambda_q(i_d, i_q) - \lambda_{qo}|\} \quad (9)$$

where, λ_{do} and λ_{qo} are inputed d and q-axis flux-linkages, respectively. λ_d and λ_q are obtained from flux maps with iterative solution of i_d and i_q.

To minimize F_{obj}, an iterative process is used to find i_d and i_q. The process continues until F_{obj} is reduced to the desired tolerance. During the process, the flux-linkages, λ_d and λ_q, are interpolated on the FEA-calculated flux maps. Fig. 4 shows the obtained d and q-axis currents (i_d, i_q).

The accuracy of inverse model is validated based on the introduced flux errors. The obtained currents (i_d, i_q), in Fig. 4, are used to estimate their corresponding flux-linkages by the interpolation on FEA-calculated flux maps. Then the obtaied flux-linkages are compared to the inputed flux-linkages that are used to generate the d- and q-axis currents. The obtained d and q-axis flux-linkage error maps are shown in Fig. 5. As noted, the maximum errors in d and q-axis flux-linkages are very samll and can be ignored. This also ensures a high accuracy of flux to current inverse solution.

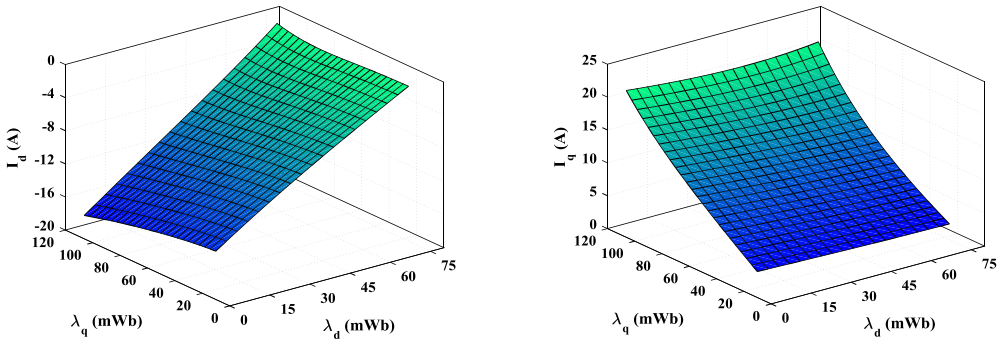

(a) (b)

Fig. 4. The current maps (a) d-axis current, (b) q-axis current.

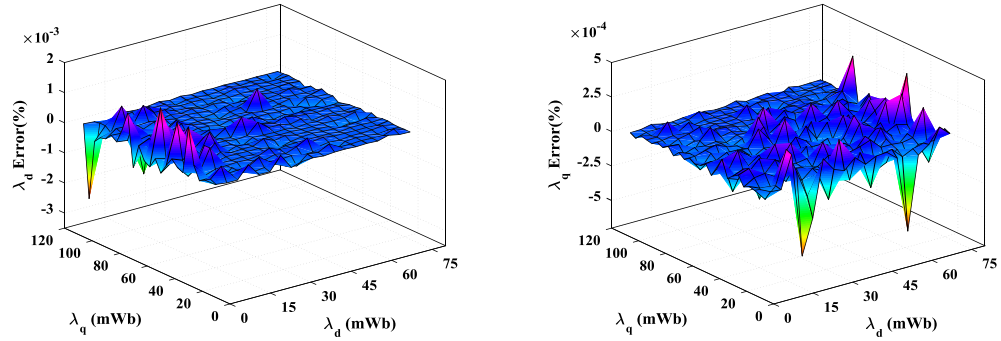

(a) (b)

Fig. 5. The flux error maps (a) d-axis flux error, (b) q-axis flux error.

3. Modeling of system losses

This section describes the total system losses that mainly include the motor losses and inverter losses.

3.1. Loss Model of PMSMs

The motor losses are copper losses, iron losses, harmonic iron losses, and mechanical loss. Thus, the total motor losses, P_{M_loss} are given by Equation (10).

$$P_{M\_loss} = P_{cu} + P_{Fe,f} + P_{Fe,h} + P_{mech} \tag{10}$$

3.1.1. Copper losses

The fundamental copper loss of an IPMSM can be estimated by Equation (10). The harmonics copper losses can be ignored as the employed switching frequency of inverter is 10kHz [7].

$$P_{cu} = 3I_s^2 R_s = \frac{3}{2} R_s \left(i_d^2 + i_q^2\right) \tag{11}$$

3.1.2. Iron losses

The Bertotti iron loss formula is a widely used method to evaluate the iron loss in electric machines. It calculates iron losses per unit volume as follows [30].

$$dP_{fe} = k_h f B_m^{\alpha} + k_c f^2 B_m^2 + k_e f^{1.5} B_m^{1.5} \tag{12}$$

where f is the frequency. B_m is the maximum value of flux density. α is a coefficient (α=2). The coefficients K_h, k_c, and k_e are for hysteresis loss, eddy current loss, and additional loss, respectively.

The coefficient of eddy current loss is calculated as in Equation (13) [6].

$$k_c = \frac{\pi^2 \sigma k_d^2}{6} \tag{13}$$

where σ is the material conductivity. k_d is the lamination thickness.

The stator iron losses are estimated using average flux density in both the yoke and tooth. The d- and q-axis fluxes ($\phi_{d,q}$) are deduced from flux-linkages as follows [8].

$$\phi_{d,q} = \frac{\sqrt{2}}{\sqrt{3}} \frac{\lambda_{d,q}}{N_T K_w} \tag{14}$$

where N_T is the number of phase turns. K_w is the winding factor.

The average flux density in tooth and yoke can be derived as given by Equation (15).

$$B_{td,q} = \frac{\phi_{d,q}}{\alpha_i A_t Q/(2p)} = \frac{\lambda_{d,q}}{A_{tc}}$$
$$B_{yd,q} = \frac{\phi_{d,q}}{2A_y} = \frac{\lambda_{d,q}}{A_{yc}} \tag{15}$$

where A_t and A_y are the physical areas of stator tooth and yoke, respectively. The A_{tc} and A_{yc} represents the equivalent areas of stator tooth and yoke, respectively. Q is the number of slots.

$$A_{tc} = \frac{\sqrt{3}}{\sqrt{2}} (N_T K_w).\alpha_i A_t Q/(2p); \quad A_{yc} = \frac{\sqrt{3}}{\sqrt{2}} (N_T K_w).2A_y \tag{16}$$

where α_i is the pole arc factor.

The iron loss as a function of flux-linkages can be calculated using Equation (17), after substituting Equation (15) into Equation (12) and multiplying the tooth and yoke volumes.

$$P_{fe} = k_1\left(\lambda_d^2 + \lambda_q^2\right) + k_2\left(\lambda_d^{1.5} + \lambda_q^{1.5}\right) \tag{17}$$

where k_1 is the coefficient of iron loss (hysteresis and eddy losses). k_2 is the coefficient of excess iron loss.

$$k_1 = (k_h f + k_c f^2)\left(\frac{V_t}{A_{tc}^2} + \frac{V_y}{A_{yc}^2}\right); \quad k_2 = k_e f^{1.5}\left(\frac{V_t}{A_{tc}^{1.5}} + \frac{V_y}{A_{yc}^{1.5}}\right) \tag{18}$$

$$V_t = Q h_t A_t; \quad V_y = \pi(D_s - h_y)A_y \tag{19}$$

where V_t and V_y are the total volumes of stator tooth and yoke**,** respectively. h_t and h_y are the heights of stator tooth and yoke, respectively. D_s is the outer diameter of stator.

Without the consideration of excess loss, the equivalent iron loss resistance R_c is given by Equation (20).

$$R_c = \left(\frac{\omega_e^2}{k_1}\right) \tag{20}$$

The magnet eddy current loss P_{mag} can be estimated using Equation (21).

$$P_{mag} = \frac{V_M\, b_M^2 B_m^2 f^2}{12\rho_M} \tag{21}$$

where V_M is the magnet volume, b_M is the magnet width, ρ_M is the magnet resistivity.

3.1.3. Harmonic iron loss

The harmonic iron loss (P_{fe_h}) occurs because of the time variation of flux density. It is calculated as a function of ripple voltage rms, ΔV_{rms}^2, DC link voltage $V_{dc,}$ and modulation index m as given by Equation (22) [31]. The modulation index is defined as $m = \frac{\sqrt{3}V_m}{V_{dc}}$.

$$P_{fe,h} = K_{h,eddy}\Delta V_{rms}^2 \tag{22}$$

$$\Delta V_{rms}^2 = \frac{V_{dc}^2}{3}\left(\frac{2}{\pi}m - \frac{1}{2}m^2\right) \tag{23}$$

where V_m is the peak output voltage. $K_{h,eddy}$ is eddy current loss coefficient and it is taken as 2.3 mW/V^2 [31].

3.1.5. Mechanical loss

Despite the mechanical losses (P_{mech}) do not affect the optimal current angle selection, it is calculated to represent the accurate system efficiency. The mechanical losses are calculated as a cubic function of speed as follows.

$$P_{mech} = K_{mech}\omega_r^3 \tag{24}$$

where, K_{mech}, is the mechanical loss coefficient.

3.2. The Inverter losses

In general, the inverter losses are categorized as conduction losses and switching losses. There is also the blocking loss that can be neglected as it is a

very small amount [32]. The used IGBT module is IM393-X6F (600V/20A) intelligent power module (IPM) from Infineon Technologies. The required data of IGBT module can be obtained from its online datasheet. The data is also given in Table 1.

3.2.1. The conduction losses

The conduction losses are like the resistive losses. It occurs because of the internal resistances of IGBTs/diodes when conducting currents. These losses depend on current level and the junction temperature. The conduction loss of one IGBT ($P_{co\text{-}IGBT}$) and conduction loss for one diode ($P_{co\text{-}diode}$) in a 2-level VSI can be defined as in Equation (25) and Equation (26), respectively.

$$P_{co\_IGBT} = \frac{1}{2}\left(V_{ceo}\frac{I_m}{\pi} + R_o\frac{I_m^2}{4}\right) + m\cos\theta\left(V_{ceo}\frac{I_m}{8} + R_o\frac{I_m^2}{3\pi}\right) \quad (25)$$

$$P_{co\_diode} = \frac{1}{2}\left(V_{Do}\frac{I_m}{\pi} + R_D\frac{I_m^2}{4}\right) - m\cos\theta\left(V_{Do}\frac{I_m}{8} + R_D\frac{I_m^2}{3\pi}\right) \quad (26)$$

where $cos\theta$ is the power factor. V_{ceo} and V_{Do} depict the threshold voltages for IGBT and diode, respectively. R_o and R_D represent the resistances of IGBT and diode, respectively.

The power factor, $cos\theta$ is calculated by Equation (27).

$$\theta = \delta + \beta; \quad \delta = tan^{-1}\left|\frac{V_d}{V_q}\right| \quad (27)$$

where δ is the load angle.

The total conduction losses of inverter can be estimated by Equation (28).

$$P_{co} = 6 * (P_{co-IGBT} + P_{co-diode}) \quad (28)$$

3.2.2. The switching losses

The switching losses are the needed amount of energy to turn-on or turn-off any electronic switch. It is a small amount of energy but due to the huge number of ON and OFF times per second, the total dissipated energy cannot be ignored. The switching losses occur in both IGBTs and diodes. These losses depend on the switching frequency, junction temperature, dc link voltage, and current level. The switching losses of one IGBT ($P_{SW\text{-}IGBT}$) and switching loss for one diode ($P_{SW\text{-}diode}$) in a 2-level VSI can be defined by Equations (29) and (30), respectively [33].

$$P_{SW-IGBT} = \frac{1}{\pi}(e_{on} + e_{off})f_s\left(\frac{V_{dc}}{V_{nom}}\right)\left(\frac{I_m}{I_{nom}}\right) \quad (29)$$

$$P_{SW-diode} = \frac{1}{\pi}e_{rr}f_s\left(\frac{V_{dc}}{V_{nom}}\right)\left(\frac{I_m}{I_{nom}}\right) \quad (30)$$

where f_s is the switching frequency. e_{on} and e_{off} are the required amount of energy to turn–on and turn–off the IGBT, respectively. e_{rr} is the required amount of energy to turn–off the diode. V_{nom} and I_{nom} are the nominal voltage and current of loss measurements, respectively.

The total switching losses of inverter can be estimated by Equation (31). The total inverter losses can be estimated by Equation (32).

$$P_{SW} = 6 * (P_{SW-IGBT} + P_{SW-diode}) \tag{31}$$

$$P_{inv\_loss} = P_{co} + P_{SW} \tag{32}$$

4. MTPA and MEPA operation of IPMSMs

The d- and q-axis current components can be written as a function of current angle β and peak current magnitude, I_m as follow.

$$i_d = -I_m \sin\beta\,; \quad i_q = I_m \cos\beta \tag{33}$$

The main objective of MTPA is to define the best current angle β corresponding to the minimum current for the same torque production. It is equivalent to the minimization of copper loss [14]. The MTPA cannot guarantee the maximum system efficiency as it neglects the iron losses, which is significant especially at high speeds. Also, MTPA does not consider inverter losses.

On the contrary, the objective of MEPA aims to determine the current angle β that maximizes the system efficiency. The efficiency optimization involves the minimization of the overall system losses considering the motor and inverter losses. The conventional MEPA control method is given by Equation (34).

$$maximize\ \eta = \frac{P_{out}}{P_{out} + P_{loss\ t}} \tag{34}$$

$$P_{out} = T_e * \omega \tag{35}$$

$$P_{loss\_t} = P_{inv\_loss} + P_{M\_loss} \tag{36}$$

where η, P_{out}, and P_{loss_t} are the system efficiency, output power, and total losses, respectively.

The voltage and current constraints in Equation (37) must be satisfied by any control method.

$$\sqrt{V_d^2 + V_q^2} \le V_{max}; \quad \sqrt{i_d^2 + i_q^2} \le I_{max} \tag{37}$$

where V_{max} and I_{max} are the maximum permissible phase voltage and phase current, respectively.

5. The Optimization procedure

The optimization procedure involves the determination of optimal current angle β corresponding to MEPA control.

5.1. The searching algorithm

For the MEPA control, the objective function is the overall system efficiency, given by Equation (34). To achieve such goal, the machine model including all the loss models as well as the inverter losses are simulated in MATLAB Simulink environment. A steady-state model is used within the search procedure to save effort and time. The steady state model is illustrated in Fig. 6. The model employees the field-oriented control (FOC) to drive the IPMSM. The inputs are the speed ω, maximum current I_m, and the current angle β. The reference d- and q-axis voltages v_d^* and v_q^* are produced by the PI current controllers. Then, they are limited according to the voltage constraints of Equation (37). After that, the space vector pulse width modulation (SVPWM) is employed to generate the switching signals (S_{abc}).

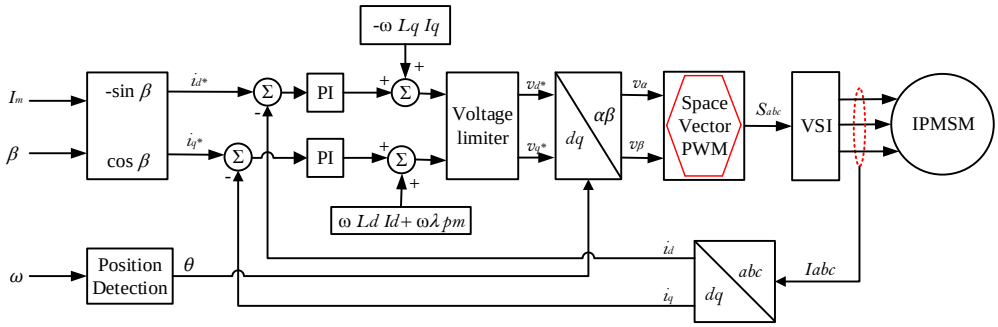

Fig. 6. The steady-state model of system including the all kinds of losses.

Fig. 7 shows the search-based procedure to determine the optimal current angle β for each operating point, defined by the given motor speed ω and maximum current I_m. First, the motor parameters based on the proposed machine model are entered, as well as the inverter loss model parameter. For a known/given motor speed ω and maximum current I_m, the current angle β are changed from its initial value ($\beta_{initial}$) to its maximum value (β_{max}) in small steps of ($\Delta\beta$). For every angle step, the simulation model is run, and the cost function (system efficiency) is estimated. Then, the current angle corresponding to MEPA is reported as the optimal angle. To develop the complete lookup table (LUT) of optimal current angles, the search procedure is repeated several times according to the desired speed and current resolutions. In this paper, the speed is changed form 250 r/min to 4500 r/min in steps of 250 r/min. The maximum current is changed form 2 A to 20 A in steps of 1 A.

Noting that the variation of current angle β from $\beta_{initial}$ to β_{max} may lead to impractical d- and q-axis current components (i_d, i_q). In this case, the motor will not track the reference d- and q-axis currents. To guarantee proper motor operation, constraints are included that ensure the current components (i_d, i_q) track their references properly. If the currents (i_d, i_q) do not track their references, the corresponding current angle is excluded from the search for optimal β. Instead of using the conventional MTPA control and the FW control of Section 4 for comparison. This paper used the searching algorithm of Fig. 7 to define the best current angles for maximum torque *production* which is equivalent to MTPA. The obtained MTPA control is much better than the conventional one as it is developed based on the proposed high-fidelity machine model. It also involves the FW control. In this case, the objective function is the torque.

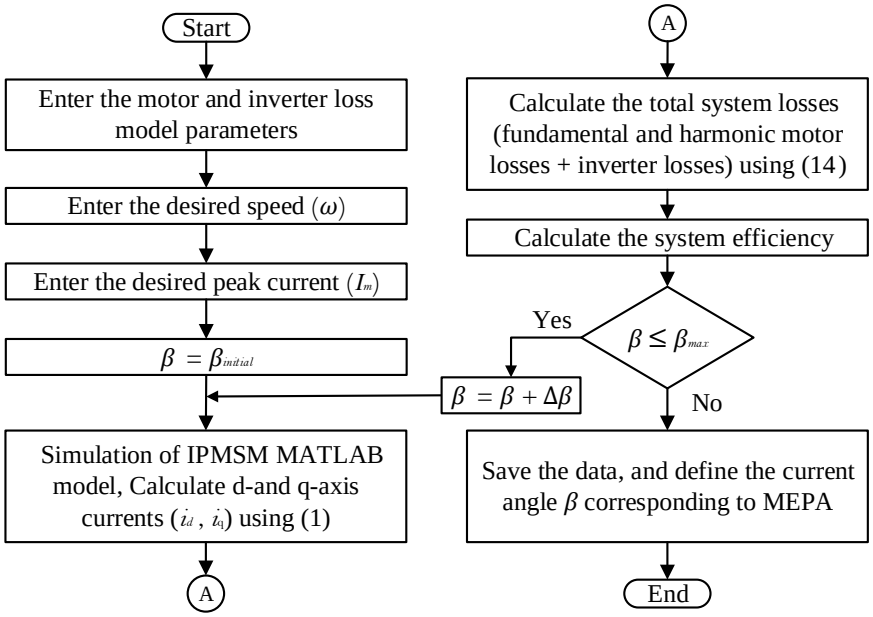

Fig. 7. Flowchart for the searching algorithm.

5.2. The optimal current angles

The obtained current angle corresponding to MEPA and MTPA are given in Fig. 8.

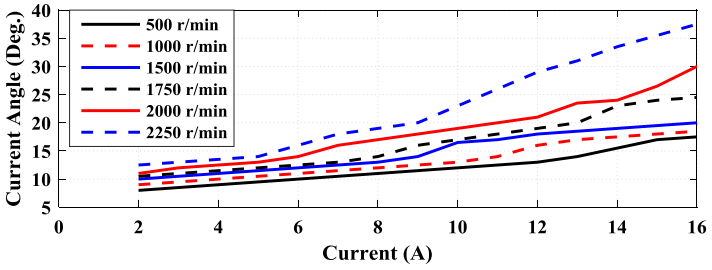

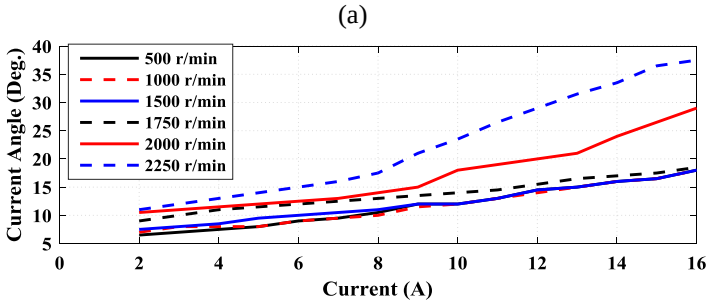

Fig. 8. The optimal current angles based on, (a) MEPA control, (b) MTPA control.

As noted, the current angle *increases* with increasing current due to the increase of iron and copper losses as well as inverter losses. Also, the current angle increases with increasing the speed because of the increase of iron loss.

The motor and system efficiencies corresponding to MEPA control are given in Fig. 9. As seen, the efficiency increases with increasing speed.

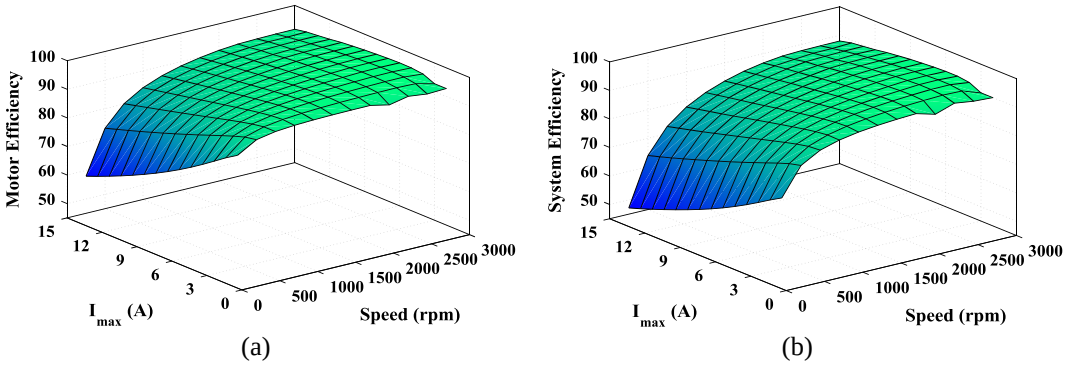

Fig. 9. The efficiency maps based MEPA control (a) motor efficiency, (b) system efficiency

6. Results and discussions

The results are divided to the steady state results and the dynamic results.

6.1. The steady-state results

Fig. 10 shows the system efficiency and output torque under the variation of current angle. As noted, the current angle greatly affects the generated torque and the system efficiency. It is also noted that the current angle corresponding to MEPA (β_{MEPA}) is different from the current angle corresponding to MTPA (β_{MTPA}). By other words, the maximum efficiency and the maximum torque do not occur at the same angles. The MEPA has a delayed current angle. For higher speed operation as in Fig. 10(b), the motor fails to operate in the range of β=0˚ to β=4˚. This is due to the essential requirement of field weakening. Hence, negative i_d current is required beyond motor base speed (1500 r/min).

Table 2 gives the system efficiencies under MTPA and MEPA controls. As noted, the drive system efficiency is the highest under MEPA control. The system efficiency is 77.67% and 77.71% for MEPA and MTPA controls, respectively. The developed torque under MEPA is 10.05 Nm which is 0.0033 Nm less than the MTPA control.

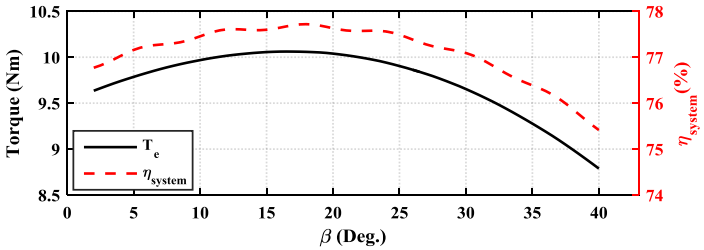

(a)

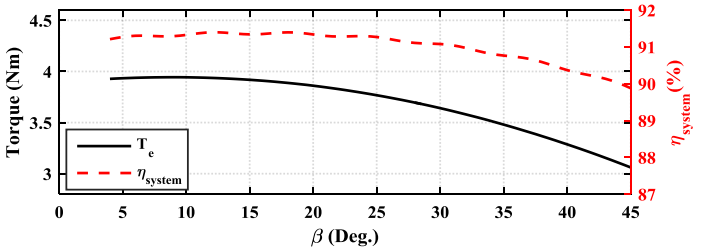

(b)

Fig. 10. The system efficiency and torque investigation through current angle sweep test at: (a) 1000 r/min and I_s = 15 A, (b) 2000 r/min and I_s = 6 A.

Table 2

Efficiency Comparison Under Each Control Strategy

	1000 r/min and Is = 15A		2000 r/min and Is =6 A	
	Efficiency	Torque	Efficiency	Torque
MTPA	77.6716	10.0616	91.2923	3.9436
MEPA	77.7192	10.0583	91.3968	3.9368

Fig. 11 shows the system efficiency and torque under different current levels. As seen, the MEPA control can provide higher efficiency. The efficiency changes with the current level as well as the speed.

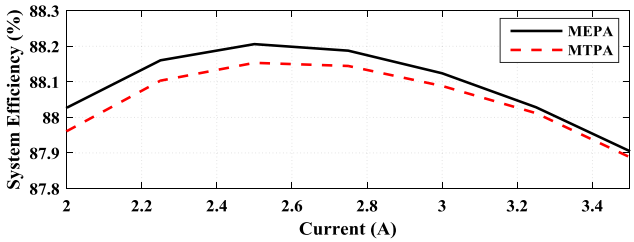

(a)

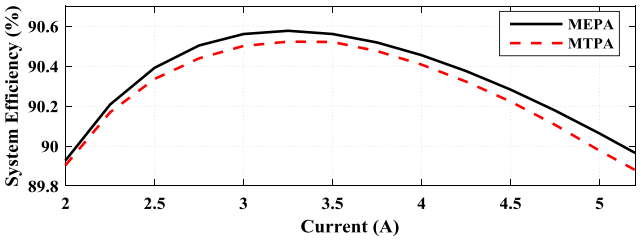

(b)

Fig. 11. The efficiency against I_m at speed of (a) 1000 r/min, (b) 1500 r/min.

6.2. The dynamic comparative studies

The implementation diagram of proposed dynamic MEPA control is done based on field-oriented control (FOC) strategy as seen in Fig. 12. The outer loop speed controller (PI) is employed to generate I_m according to with speed error $\Delta\omega$. The optimal current angles (β_{MEPA} or β_{MTPA}) are selected from LUTs as functions of ω and I_m. Hence, the reference d- and q-axis currents i_d^* and i_q^* are estimated. The dynamic comparative study between MEPA and MTPA is conducted at different speeds and EV loading. The comparison between developed MEPA and MTPA control is given in Fig. 13-15.

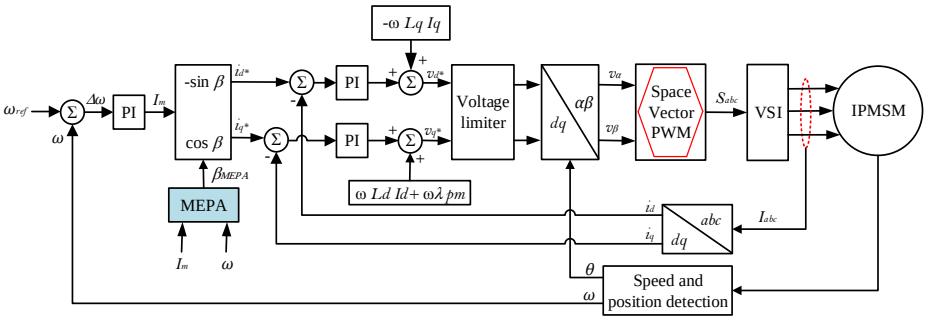

Fig. 12. The implementation diagram of proposed MEPA control.

The motor speed, torque, and reference current curves are given in Fig. 13. The reference speed is changed suddenly from 750 r/min to 1500 r/min at 0.15 sec, then to 3000 r/min at 0.3 sec as seen in Fig. 13(a). For the two control strategies, the motor has a good tracking capability to its reference speed.

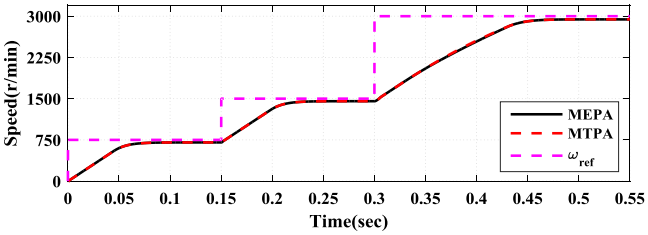

(a) The motor speed

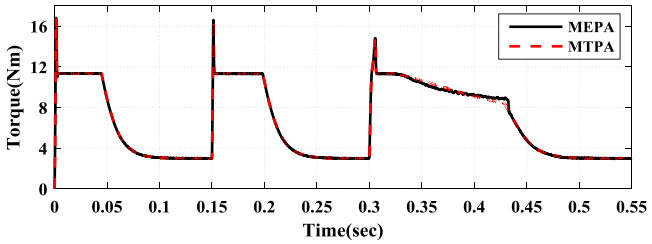

(b) The electromagnetic torque

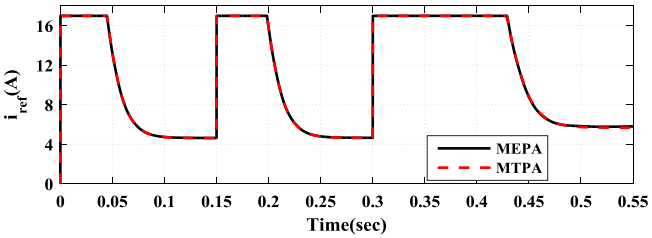

(c) The refrance current

Fig. 13. The simulation results under dynamic state.

The direct and quadrature currents as well as current angle are given in Fig. 14(a-c). As noted, the direct current with MEPA control is lower than its corresponding one for MTPA control as shown in Fig. 14(a). There is no big difference for the quadrature current as it is determined by commanded torque as shown in Fig. 14(b). Fig. 14(c) shows the current angle profile. A clear difference is observed under low-speed and light-load operations. Fig. 15 shows the motor and system efficiencies. As noted, the MEPA control provides the higher motor efficiency as well as the higher system efficiency. This is very clear by the zooming curves over motor and system efficiencies in Figs. 15(b, d), respectively.

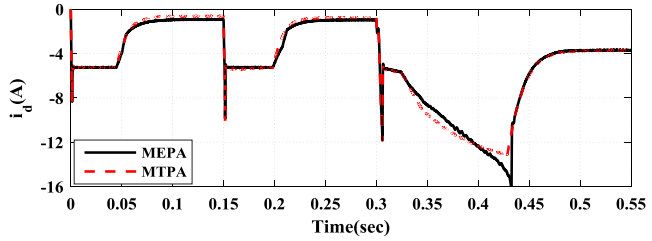

(a) The direct axis current

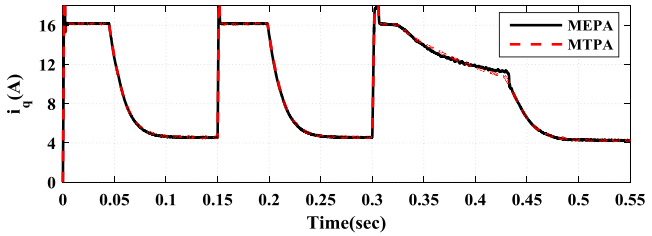

(b) The qudrature axis current

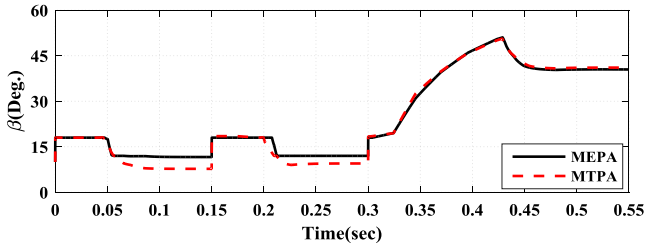

(c) The current angle

Fig. 14. The efficiency curves

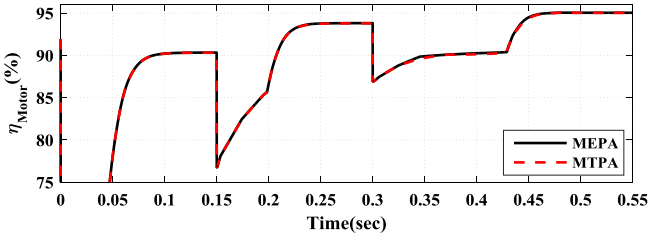

(a) The motor efficiency

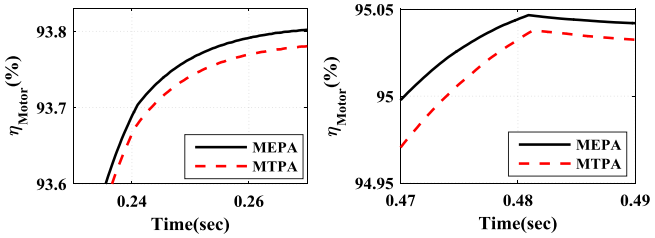

(b) Zoom on motor efficiency

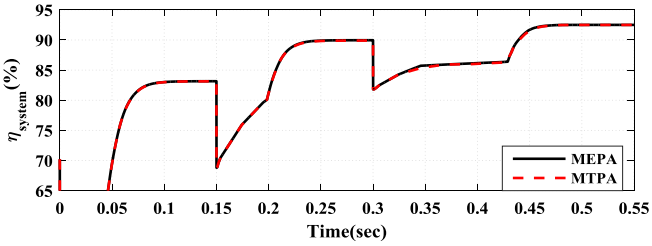

(c) The total efficiency

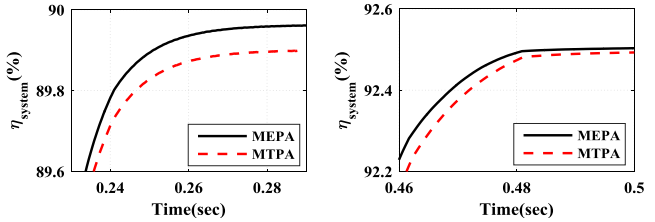

(d) Zoom on total efficiency

Fig. 15. The efficiency curves

7. Conclusions

This paper presents a MEPA control of an IPMSM over the entire speed range for EV propulsion. The overall system efficency is estimated accurately considering all the system losses. The magnetic saturation and spatial harmonic effects are considered as well as the iron loss effect. The FEA is employed to calculate the magnetic characteristics of simulated 12/10 IPMSM. The optimal current angle for MEPA operation is defined through a developed searching algorithm. Besides, the optimal current angle for MTPA operation is also defined. A comparison is conducted between the MEPA control and MTPA control. The results show the superior performance of MEPA control. The MEPA control can provide higher system efficiency compared to MTPA control at low-speed and light-load operations. It also provides better system efficiency under higher speeds due to the high iron losses which is neglected by MTPA control.

REFERENCES

[1]. *C. Lai, G. Feng, J. Tian, Z. Li, Y. Zuo, A. Balamurali, and N. C. Kar*, "PMSM Drive System Efficiency Optimization Using a Modified Gradient Descent Algorithm with Discretized Search Space," IEEE Trans. Transp. Electrif., **vol. 6**, no. 3, Sep. 2020, pp. 1104–1114.

[2]. *A. Balamurali, G. Feng, C. Lai, J. Tjong, and N. C. Kar*, "Maximum efficiency control of PMSM drives considering system losses using gradient descent algorithm based on DC power measurement," IEEE Trans. Energy Convers., **vol. 33**, no. 4, Dec. 2018pp. 2240–2249.

[3]. *J. Wu, J. Wang, C. Gan, Q. Sun, and W. Kong*, "Efficiency Optimization of PMSM Drives Using Field-Circuit Coupled FEM for EV/HEV Applications," IEEE Access, **vol. 6**, Mar. 2018, pp. 15192–15201.

[4]. *L. Dang, N. Bernard, N. Bracikowski, and G. Berthiau*, "Design Optimization with Flux Weakening of High-Speed PMSM for Electrical Vehicle Considering the Driving Cycle," IEEE Trans. Ind. Electron., **vol. 64**, no. 12, Dec. 2017, pp. 9834–9843.

[5]. *V. Ruuskanen, J. Nerg, M. Rilla, and J. Pyrhonen*, "Iron Loss Analysis of the Permanent-Magnet Synchronous Machine Based on Finite-Element Analysis over the Electrical Vehicle Drive Cycle," IEEE Trans. Ind. Electron., **vol. 63**, no. 7, Jul. 2016, pp. 4129–4136.

[6]. *Q. Chen, D. Liang, S. Jia, Q. Ze, and Y. Liu*, "Loss Analysis and Experiment of Fractional-Slot Concentrated-Winding Axial Flux PMSM for EV Applications," in 2018 IEEE Energy Conversion Congress and Exposition, ECCE 2018, Dec. 2018, pp. 4329–4335.

[7]. *A. Balamurali, G. Feng, A. Kundu, H. Dhulipati, and N. C. Kar*, "Noninvasive and Improved Torque and Efficiency Calculation Toward Current Advance Angle Determination for Maximum Efficiency Control of PMSM," IEEE Trans. Transp. Electrif., **vol. 6**, no. 1, Mar. 2020, pp. 28–40.

[8]. *R. Ni, D. Xu, G. Wang, L. Ding, G. Zhang, and L. Qu*, "Maximum Efficiency per Ampere Control of Permanent-Magnet Synchronous Machines," IEEE Trans. Ind. Electron., **vol. 62**, no. 4, 2015, pp. 2135–2143.

[9]. *C. T. Krasopoulos, M. E. Beniakar, and A. G. Kladas*, "Multicriteria PM motor design based on ANFIS evaluation of EV driving cycle efficiency," IEEE Trans. Transp. Electrif., **vol. 4**, no. 2, Jun. 2018, pp. 525–535.

[10]. *C. Lu, S. Ferrari, and G. Pellegrino,* "Two Design Procedures for PM Synchronous Machines for Electric Powertrains," IEEE Trans. Transp. Electrif., **vol. 3,** no. 1, Mar. 2017, pp. 98–107.

[11]. *H. Wang, C. Li, G. Zhang, Q. Geng, and T. Shi,* "Maximum Torque per Ampere (MTPA) Control of IPMSM Systems Based on Controller Parameters Self-Modification," IEEE Trans. Veh. Technol., **vol. 69**, no. 3, Mar. 2020, pp. 2613–2620.

[12]. *K. Li and Y. Wang,* "Maximum Torque per Ampere (MTPA) Control for IPMSM Drives Based on a Variable-Equivalent-Parameter MTPA Control Law," IEEE Trans. Power Electron., **vol. 34**, no. 7, Jul. 2019, pp. 7092–7102.

[13]. *T. Windisch and W. Hofmann*, "A novel approach to MTPA tracking control of AC drives in vehicle propulsion systems," IEEE Trans. Veh. Technol., **vol. 67**, no. 10, Oct. 2018, pp. 9294–9302.

[14]. *C. Lai, G. Feng, K. Mukherjee, J. Tjong, and N. C. Kar*, "Maximum Torque per Ampere Control for IPMSM Using Gradient Descent Algorithm Based on Measured Speed Harmonics," IEEE Trans. Ind. Informatics, **vol. 14**, no. 4, Apr. 2018, pp. 1424–1435.

[15]. *K. Liu, Q. Zhang, J. Chen, Z. Q. Zhu, and J. Zhang*, "Online multiparameter estimation of nonsalient-pole PM synchronous machines with temperature variation tracking," IEEE Trans. Ind. Electron., **vol. 58**, no. 5, May 2011, pp. 1776–1788.

[16]. *Q. Liu and K. Hameyer*, "High-Performance Adaptive Torque Control for an IPMSM with Real-Time MTPA Operation," IEEE Trans. Energy Convers., **vol. 32**, no. 2, Jun. 2017, pp. 571–581.

[17]. *T. Sun, J. Wang, and M. Koc*, "Virtual Signal Injection-Based Direct Flux Vector Control of IPMSM Drives," IEEE Trans. Ind. Electron., **vol. 63**, no. 8, Aug. 2016, pp. 4773–4782,

[18]. *T. Sun, J. Wang, and M. Koc,* "On Accuracy of Virtual Signal Injection based MTPA Operation of Interior Permanent Magnet Synchronous Machine Drives," IEEE Trans. Power Electron., **vol. 32**, no. 9, Sep. 2017, pp. 7405–7408.

[19]. *B. Chen, A. Shen, X. Luo, Z. Dou, and P. Luo*, "Novel MTPA control strategy for IPMSM based on multiple virtual signals injection," IET Electr. Power Appl., vol. 14, no. 3, Mar. 2020, pp. 457–463.

[20]. *Z. Li and H. Li ,*"MTPA control of PMSM system considering saturation and cross-coupling", in 2012 15th International Conference on Electrical Machines and Systems (ICEMS), Oct. 2012.

[21]. *P. Dück and B. Ponick*, "A novel iron-loss-model for permanent magnet synchronous machines in traction applications," in 2016 International Conference on Electrical Systems for Aircraft, Railway, Ship Propulsion and Road Vehicles & International Transportation Electrification Conference (ESARS-ITEC), Nov. 2016.

[22]. *P. H. Mellor, R. Wrobel, and D. Holliday*, "A computationally efficient iron loss model for brushless AC machines that caters for rated flux and field weakened operation," in 2009 IEEE International Electric Machines and Drives Conference, IEMDC '09, 2009, pp. 490–494.

[23]. *H. Sano, K. Narita, T. Asanuma, and T. Yamada*, "An accurate iron loss evaluation method based on Finite Element Analysis for Permanent Magnet Motors," in Proceedings - 2016 22nd International Conference on Electrical Machines, ICEM 2016, Nov. 2016, pp. 1284–1289.

[24]. *M. N. Uddin and R. S. Rebeiro*, "Online efficiency optimization of a fuzzy-logic-controller-based IPMSM drive," IEEE Trans. Ind. Appl., **vol. 47**, no. 2, Mar. 2011, pp. 1043–1050.

[25]. *S. Yang, K. Liu, Y. Hu, L. Chu, and S. Chen*, "Efficiency optimization control of IPMSM considering varying machine parameters," in 2018 IEEE Student Conference on Electric Machines and Systems, Dec. 2018

[26]. *K. Zhang, T. Sun, G. Xie, J. Zhang, G. Xiong, J. Liang, and S. He*, "High-Fidelity Model for Interior Permanent Magnet Synchronous Machines Considering the Magnet Saturation and Spatial Harmonics Based on Deep Neural Network," in 2019 22nd International Conference on Electrical Machines and Systems (ICEMS), Aug. 2019.

[27]. *X. Chen, J. Wang, B. Sen, P. Lazari, and T. Sun*, "A high-fidelity and computationally efficient model for interior permanent-magnet machines considering the magnetic saturation, spatial harmonics, and iron loss effect," IEEE Trans. Ind. Electron., **vol. 62**, no. 7, Jul. 2015, pp. 4044–4055.

[28]. *S. Li, D. Han, and B. Sarlioglu*, "Modeling of Interior Permanent Magnet Machine Considering Saturation, Cross Coupling, Spatial Harmonics, and Temperature Effects," IEEE Trans. Transp. Electrif., **vol. 3**, no. 3, Sep. 2017, pp. 682–693.

[29]. *Y.-M. You*, "Optimal Design of PMSM Based on Automated Finite Element Analysis and Metamodeling," Energies, **vol. 12**, no. 24, Dec. 2019, p. 4673.

[30]. *D. Lin, P. Zhou, W. N. Fu, Z. Badics, and Z. J. Cendes*, "A dynamic core loss model for soft ferromagnetic and power ferrite materials in transient finite element analysis," in IEEE Transactions on Magnetics, **vol. 40**, no. 2 II, Mar. 2004, pp. 1318–1321.

[31]. *M. Schweizer, T. Friedli, and J. W. Kolar*, "Comparative evaluation of advanced three-phase three-level inverter/converter topologies against two-level systems," IEEE Trans. Ind. Electron., **vol. 60**, no. 12, 2013, pp. 5515–5527.

[32]. *M. Saur, B. Piepenbreier, W. Xu, and R. D. Lorenz*, "Implementation and evaluation of inverter loss modeling as part of DB-DTFC for loss minimization each switching period," in 2014 16th European Conference on Power Electronics and Applications, Sep. 2014.

[33]. *J. Guo*, "Modeling and Design Of Inverters Using Novel Power Loss Calculation And Dc-Link Current/Voltage Ripple Estimation Methods And Bus Bar Analysis - Google Search," McMaster University, 2017.